Journal of Nuclear Materials 384 (2009) 1–5

Contents lists available at ScienceDirect

Journal of Nuclear Materials

journal homepage: www.elsevier.com/locate/jnucmat

Creep behavior of oxide dispersion strengthened 8Cr–2WVTa and 8Cr–1W steels

K. Shinozuka [a,*], M. Tamura [a], H. Esaka [a], K. Shiba [b], K. Nakamura [b]

[a] Department of Material Science and Engineering, National Defense Academy, Yokosuka, Kanagawa 239-8686, Japan
[b] Japan Atomic Energy Agency, Tokai-mura, Naka-Gun, Ibaraki 319-1195, Japan

ARTICLE INFO

PACS:
81.40.Lm

ABSTRACT

Microstructures and creep behavior of two martensitic oxide dispersion strengthened (ODS) steels 8%Cr–2%W–0.2%V–0.1%Ta (J1) and 8%Cr–1%W (J2) with finely dispersed $Y_2Ti_2O_7$ have been investigated. Creep tests have been carried out at 670, 700 and 730 °C. Creep strength of J1 is stronger than that of any other ODS martensitic steels and the hoop strength of the ferritic ODS steel cladding. At the beginning of creep test, shrinkage was frequently observed for J1. This is one of the reasons for high creep strength of J1. The δ-ferrite, which is untransformed to austenite at hot isostatic press and hot rolling temperatures, was elongated along the rolling direction, and volume fraction of δ-ferrite in J1 is larger than J2. Although the elongated δ-ferrite affects the anisotropy of creep behavior, the extent of anisotropy in J1 is not so large as that of the ferritic ODS steel.

1. Introduction

Construction of International Thermonuclear Experimental Reactor (ITER) is planned. Its Test Blanket Modules in Japan will consist of F-82H steel which is 8Cr–2WVTa reduced activation martensitic steel [1]. Application of oxide dispersion strengthened (ODS) steel in the first wall is studied for the further development of a nuclear fusion reactor. The 9–14%Cr ODS steels have been recently studied, because the ODS steels are expected to be used at higher temperatures than 650 °C [2–4]. However, the ODS products exhibit lower toughness than the usual reduced activation ferritic/martensitic steels without fine dispersed oxides [5]. Ductile-brittle-transition-temperature is improved by making a very fine microstructure in MA957 [6]. However, ODS steel had anisotropy in thermal creep resistance and toughness. Ukai et al. applied the special recrystallizing method to the ODS steel to solve the problem [2,7–9]. The method of improving the anisotropy was also examined by using martensitic structure in lower Cr concentration [7].

Some of the authors, Shiba and Nakamura, have studied the ODS steel composed of 8%Cr–2%W–0.2%V–0.1%Ta, ODS steel (J1) which is identical to the reduced activation martensitic steel, F-82H, except for Y_2O_3, titanium and excess oxygen. They have also studied the higher toughness ODS steels which has fixed Cr concentration of 8% with W concentration varying from 0% to 3%, and they have concluded that 8%Cr–1%W ODS steel (J2) shows better toughness [10]. The objective of this study is to investigate the thermal creep strength along the hot rolling direction and the transverse direction of rolled plates of the 8%Cr–2%W–0.2%V–0.1%Ta ODS steel (J1) and 8%Cr–1%W ODS steel (J2).

2. Experimental procedure

Two kinds of materials J1 and J2 were prepared and their chemical compositions are shown in Table 1. Mixed metallic and Y_2O_3 powders were mechanically alloyed in Ar gas atmosphere. Complex oxide, $Y_2Ti_2O_7$, was formed from Y_2O_3, Ti and O supplied by impurity in Ar gas and surface contamination on powders during mechanical alloying [7,8]. Excess O content is shown in Table 1. The mechanical alloyed powders were encapsulated and degassed in vacuum at 400 °C for 3 h. The capsule was hot isostatic pressed (HIPed) at 190 MPa and 1150 °C for 1 h, and then rolled from 60 mm to 20 mm in thickness at 1100 °C. The rolled plates was normalized at 1050 °C for 1 h and then tempered at 750 °C for 1 h.

Creep test specimens were sampled along the hot rolling direction and the transverse direction. The machined specimens had a diameter of 5 mm and gauge length of 25 mm. The surface of the gauge area was polished with SiC polishing papers in grit sizes ranging up to #4000. Creep tests were carried out at 670, 700 and 730 °C in the stress range of 143–228 MPa.

Microstructural analyses were made on the normalized and tempered condition by using an optical microscope (OM) and a field emission transmission electron microscope (FE-TEM) equipped with energy dispersive X-ray (EDX) analyzer. Specimens for OM observation were etched with a dilute solution of 1% picric acid and 4% hydrochloric acid in methanol to identify δ-ferrite grains. For FE-TEM observation, thin foil was prepared by a twin-jet electropolishing apparatus using a dilute solution of 25% nitric

* Corresponding author. Tel.: +81 46 841 3810; fax: +81 46 844 5910.
E-mail address: kshinozu@nda.ac.jp (K. Shinozuka).

0022-3115/$ - see front matter © 2008 Elsevier B.V. All rights reserved.
doi:10.1016/j.jnucmat.2008.09.006

Table 1
Chemical compositions of J1 and J2

	C	Cr	W	V	Ta	Y_2O_3	Ti	Ex. O
J1	0.16	7.85	1.90	0.18	0.10	0.368	0.19	0.092
J2	0.16	8.05	1.01	<0.01	<0.01	0.381	0.20	0.089

Fe for the balance.
'Ex. O' was calculated by subtracting the amount of the oxygen contained in Y_2O_3 from the total amount of oxygen in a specimen (mass%).

acid in methanol at −30 °C. Vickers hardness tests were also performed.

To identify precipitates, each specimen was electrolyzed in a 10% acetyl acetone-1% tetramethyl ammonium chloride–methanol electrolyte solution (10% AA solution) and the residue was separated using a filter having 0.1 μm pores. The residue along with the filter was analyzed by X-ray diffraction (XRD) method.

3. Results and discussion

3.1. Microstructures

Fig. 1 shows optical micrographs of longitudinal section of J1 (J1-L), transversal section of J1 (J1-T), longitudinal section of J2 (J2-L) and transversal section of J2 (J2-T). J1 and J2 indicated the tempered martensitic structure. Whitish looking grains in Fig. 1 were untransformed ferritic grains which were produced during hot isostatic pressing (HIP). The untransformed ferritic grains are elongated along the hot rolling direction. The similar grains are also seen into the alloy of 9Cr–ODS martensitic steel for the fuel pins cladding [9,11]. Ukai et al. have explained as follows: the grains could be non-transformed α phase that were not transformed during normalizing, and these α grains are not equilibrium δ-ferrite phase at normalizing temperature. Nevertheless, the untransformed ferritic grains are called δ-ferrite in this paper, because they were in equilibrated state at the HIP temperature, the hot-rolling temperature and the normalizing temperature. The area fraction was calculated with the image analysis software using optical micrographs, and this is considered as the volume fraction. The volume fraction of δ-ferrite of J1 and J2 are about 15% and 10%, respectively.

The TEM images of J1 and J2 are shown in Fig. 2. Small particles of 5–15 nm in diameter are observed in both photographs. Large elliptical particles of around 50 nm in the major axis were also observed in J1. According to the XRD analysis of each extracted residue of J1 and J2, precipitates found in both of J1 and J2 are $Cr_{23}C_6$, $Y_2Ti_2O_7$, Y_2O_3 and Ti_2O_3. Tantalum carbide could not be detected in the J1 specimen. Large elliptic particles were judged to be $Cr_{23}C_6$ since large amount of Cr was detected by EDX analysis. They are finer than the usual martensitic heat resistant steels where their size is typically 130 nm in normalized and tempered condition [12]. Furthermore, yttrium and titanium enrichments were observed in small particles, thus small particles were considered to be $Y_2Ti_2O_7$ or other Y–Ti complex oxides. The particles of Y_2O_3 and Ti_2O_3 were not identified by FE-TEM and EDX.

Results of Vickers hardness tests using 10 kg load in the normalized and tempered condition of J1 and J2 were 416 and 379, respectively. These are twice the value of F82-H in the normalized-and-tempered condition, and are almost the same as the value of F82-H in the normalized condition [12,13]. In general, ODS steels exhibit high Vickers hardness [14].

3.2. Creep rupture properties

All results of creep rupture test are showed in Fig. 3. Stress is plotted as a function of logarithm of time to rupture. This semi-log plot is based on the relation:

$$t_r = t_{r_0} \exp\left(\frac{Q - \sigma V}{RT}\right), \tag{1}$$

where t_r is time to rupture, t_{r_0} is the pre-exponential factor, Q is the apparent activation energy, σ is stress, V is the activation volume, R is the gas constant and T is absolute temperature [15]. In addition, $-\log t_{r_0}$ is equivalent to the Larson–Miller constant (C), which is usually assumed to be 20. This semi-log plot is advantageous for comparison of data vis-a-vis the conventional log–log plot, because semi-log plots for many other of heat resistant steels have shown a

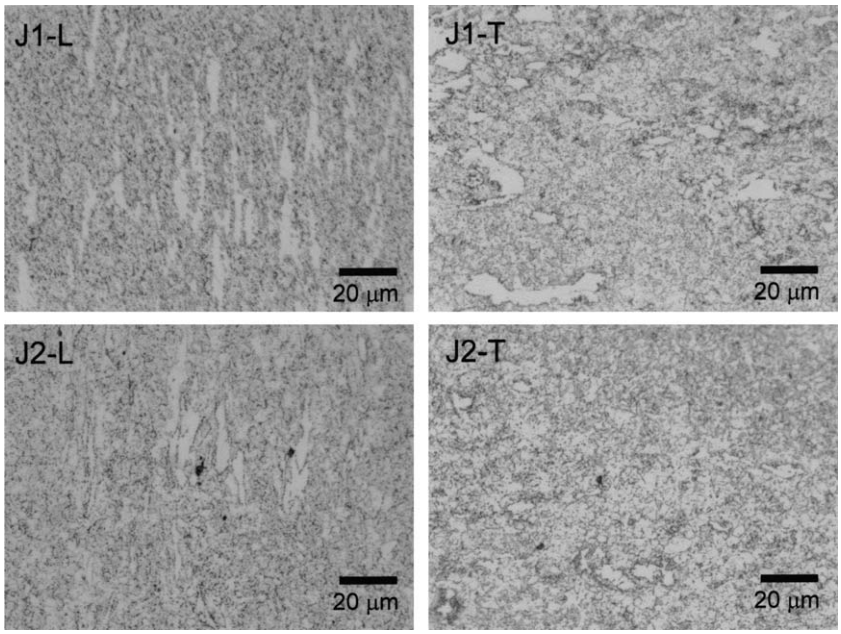

Fig. 1. Optical micrographs of cross-section of J1 and J2 as normalized and tempered condition. J1-L and J2-L are longitudinal section and J1-T and J2-T are the transverse section. The rolling direction is the up-and-down direction of a photograph about J1-L and J2-L, and is a perpendicular direction of a photograph about J1-T and J2-T.

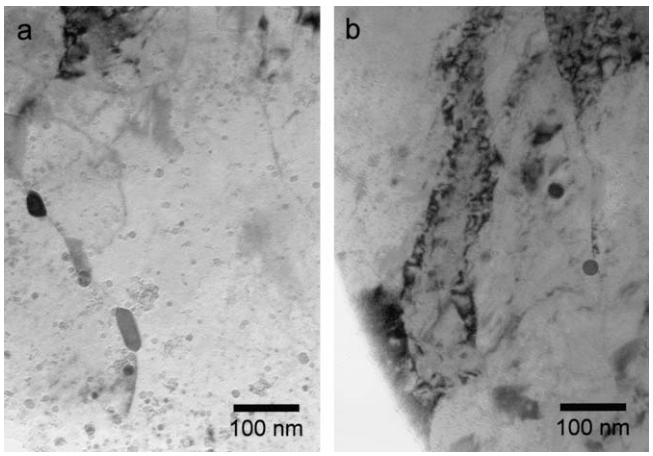

Fig. 2. Typical high resolution TEM images of J1 (a) and J2 (b).

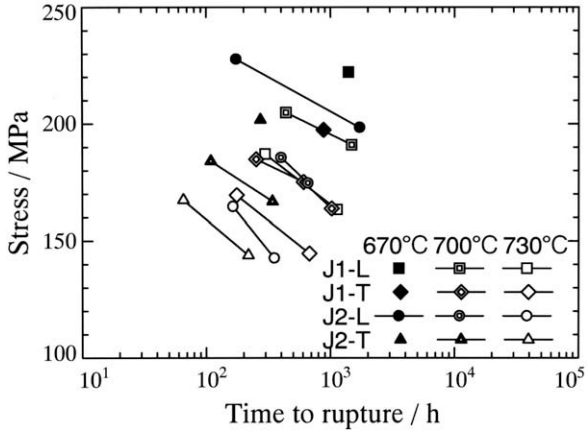

Fig. 3. Stress as a function of logarithm of time to rupture. '-L' and '-T' indicate that the direction of load is parallel and perpendicular to the rolling direction, respectively.

linear relationship for a wide range of time to rupture. The numerical values of Q, V and t_{r_0} which were calculated from the time to rupture and stress of each sample are shown in Table 2. Using these values we can easily estimate creep strength for different temperatures and time.

J1-L had the longest time to rupture at each temperature, on the other hand J2-T had the shortest. At 670 °C the time to rupture of J2-L was more than J1-T, but the time to rupture of J2-L was lesser than J1-T at 730 °C. Nevertheless, the ratio of time to rupture of J1-L to J1-T was similar to that of J2-L to J2-T in temperature range of 670–730 °C. These results mean that J1 was stronger than J2 and that each longitudinal strength was more than the respective transverse strength. The anisotropy of the time to rupture of J1 and J2 was relatively small when compared to the ferritic ODS steel [16], and this issue will be discussed in a later section.

Creep curves for J1 and J2 at 700 °C are shown in Fig. 4. The stresses for J1-L, J1-T, J2-L and J2-T are 191 MPa, 185 MPa, 186 MPa and 184 MPa, respectively. The creep curves of J2 in Fig. 4 indicate the usual curves and elongation at rupture was larger than 1%. However, shrinkage was observed for J1 immediately after loading and rupture elongation of J1 was small as shown in Fig. 4. In other experimental conditions too, a similar phenomenon was observed for J1. Shrinkage phenomenon during creep was also reported in Fe–0.11%Ta–0.014%C alloy and Fe–0.17%Ta–0.016%C alloy and the shrinkage caused the increase in creep strength [17]. This phenomenon is explained as follows: dislocations drag C and Ta form fine particles of TaC, and these particles cause not only increase in creep resistance but also the decrease in lattice constant of the matrix due to the consumption of interstitial atom of carbon. In the same way if TaC precipitated in J1, it would lead to a shrinkage and result in higher creep strength than J2. During XRD analysis of extracted residue of J1, TaC could not be detected and this could be due to the very small TaC particles not getting trapped in the filter. Furthermore, since the concentration of tungsten in J1 is higher than J2, it is supposed that higher strength in J1 was owing to the solid solution strengthening by tungsten.

Table 2
Q, V and t_{r_0} calculated from the time to rupture and stress of each sample

	J1-L	J1-T	J2-L	J2-T
Q/kJ mol^{-1}	610.2	488.0	458.1	432.2
V/cm^3 mol^{-1}	542.9	492.6	268.7	418.1
t_{r_0}/h	7.958×10^{-25}	1.334×10^{-19}	4.762×10^{-20}	8.500×10^{-18}

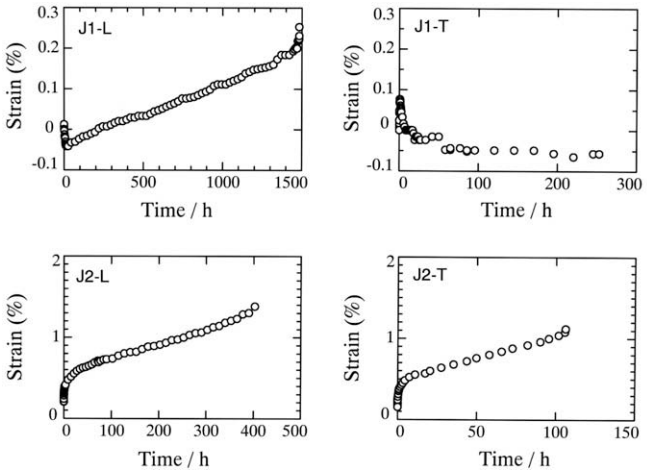

Fig. 4. Strain as a function of time of J1-L, J1-T, J2-L and J2-T at 700 °C in the stress range of 184–191 MPa.

3.3. Deformation

In general, superior creep strength of the ODS steels are caused by finely dispersed Y–Ti complex oxide particles and fine precipitation of $Cr_{23}C_6$ [12,13]. It seems difficult to explain the observed anisotropy in the creep strength by only the dispersion of oxide particles, because high resolution TEM images showed the uniform dispersion of the complex oxides. J1 had more volume fraction of δ-ferrite than J2, and creep strength of J1 was higher. Therefore, it was considered that the arrangement of the δ-ferrite grains should be related to the anisotropy of the creep strength.

The cross-sectional optical microscopic photographs near the fracture plane are shown in Fig. 5 for the respective specimens of Fig. 4. The micrograph magnified near the voids in J1-L is also presented in Fig. 6. In J1-L, it is observable that voids were formed in martensitic structure along the elongated δ-ferrite grains. A similar microstructure is confirmed in MA957 [18]. Since voids were formed along the loading direction, it is not considered that individual clusters of the δ-ferrite effectively assisted in propagation of a main crack for rupture and thus the voids caused decrease in creep strength. On the other hand, in J1-T, since a main crack for rupture was parallel to the elongated δ-ferrite grains, the crack propagated along the voids as shown in Fig. 7, which caused the

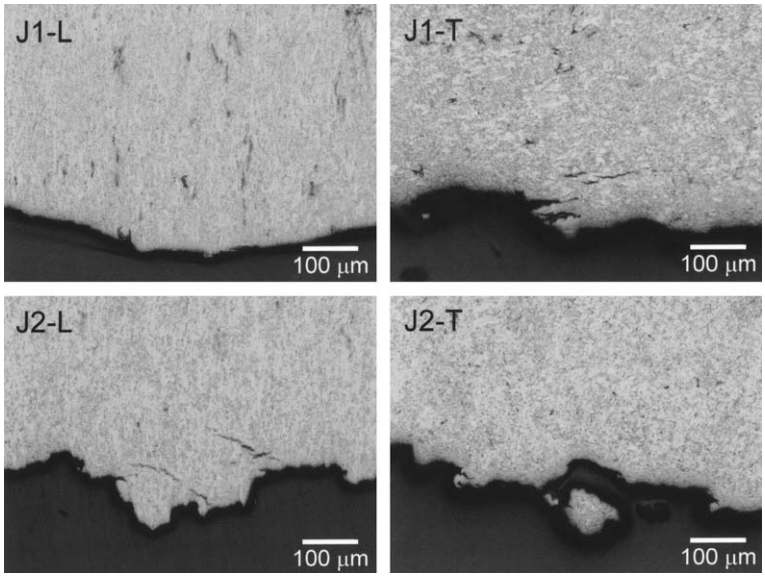

Fig. 5. Optical micrographs of cross-section near fracture surface of J1-L, J1-T, J2-L and J2-T. The direction of load is the up-and-down direction of photographs.

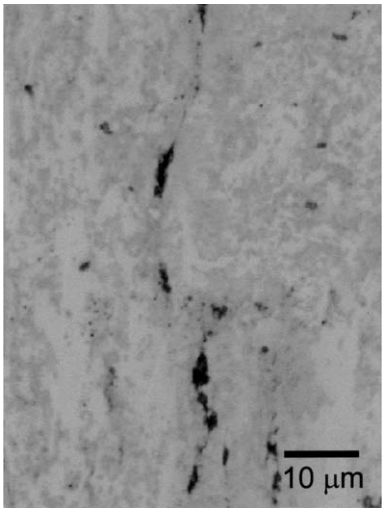

Fig. 6. Optical micrograph of the ruptured J1-L, forming voids in the martensite structure along the elongated δ-ferrite grains.

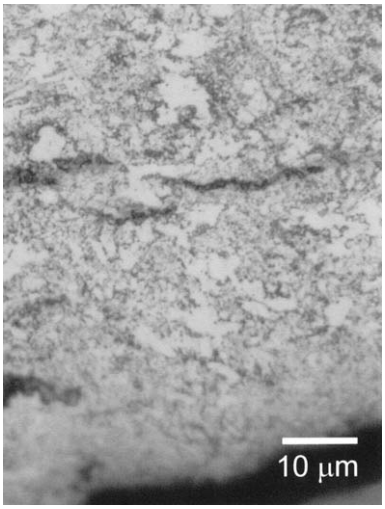

Fig. 7. Optical micrograph of the ruptured J1-T. The crack is parallel to the elongated δ-ferrite grains and propagated along the voids.

decrease in creep strength. Difference in crack propagation direction in relation to the δ-ferrite caused the anisotropy of creep strength. Although voids were formed in martensite along the δ-ferrite grains in J2-L the amount of voids formed was small in J2, since the volume fraction of δ-ferrite was low. It also seems that small arrays of voids assisted the propagation of main crack for rupture in J2-T.

In comparison between the creep strength of the ferritic ODS steels and the martensitic ODS steels, it is reported that the ferritic ODS steel are stronger than the martensitic ODS steel [6,9,18–20]. If this is applicable to J1 and J2, deformability of δ-ferrite is less than that of the matrix. Therefore, difference in the deformability between the δ-ferrite and matrix caused the formation of voids at boundaries as shown in Fig. 6.

Since FE-TEM observations show that J1 and J2 were roughly comparable in the size and dispersing condition of fine dispersed oxide particles and $Cr_{23}C_6$. Therefore, the contribution of these precipitates to creep strength would be practically equal for J1 and J2. One of the reasons that the creep strength of J1 was stronger than J2 was the dynamic formation of TaC at the beginning of creep deformation and the finely formed TaC. Moreover, the volume fraction of δ-ferrite and the solid solution strengthening by tungsten in J1, which was larger than J2, would contribute towards higher creep strength in J1. For improving martensitic ODS steels, systematic research by changing the volume fraction of δ-ferrite, is necessary.

3.4. Creep strength with the literature data

It has been established that Eq. (1) is applicable to creep rupture data, and it is easy to estimate the time to rupture for longer time using this relation [15]. Fig. 8 shows the estimated stresses at 650 °C for J1 and J2 by broken lines as a function of logarithm of time to rupture from data of Table 2, since a lot of rupture tests of the heat-resisting alloys have been made at 650 °C. Fig. 8 also indicates the published creep strength at 650 °C for the ODS steels [6,9,19,20] and the superior heat resistant steels by melting process [21,22]. The data for ODS-Eurofer with 0.5% Y_2O_3 were

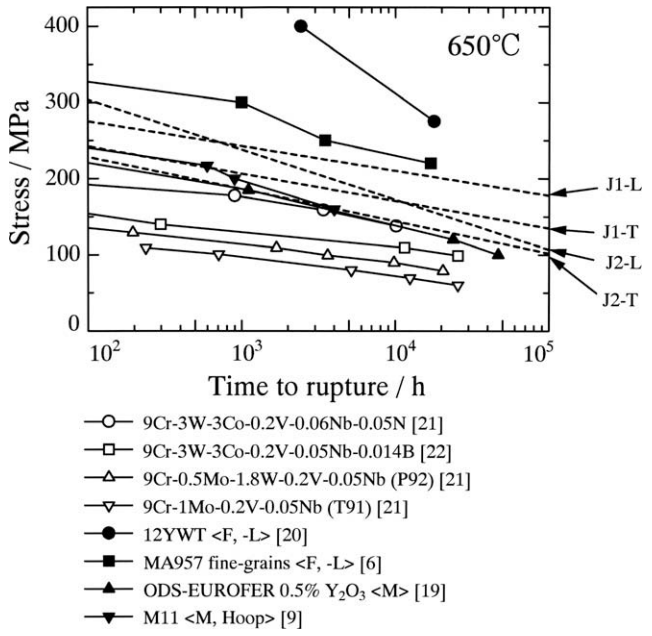

Fig. 8. Stress as a function of logarithm of time to rupture with other high creep strength materials at 650 °C. Broken lines of J1-L, J1-T, J2-L and J2-T were estimated from creep data at 670, 700 and 730 °C. 'F' and 'M' mean a ferrite and a martensite, respectively. '-L' means that the direction of load is parallel to the rolling direction, and 'Hoop' means the hoop stress by a tube.

converted to the time to rupture at 650 °C from the values of the Larson–Miller parameter at temperatures between 600 and 700 °C [19]. Even J2-T the weakest among our specimens is stronger than the famous heat resistant steels made by melting process including the alloy studied by Taneike et al. [21] and is comparable as the martensitic ODS steels, such as ODS-Eurofer with 0.5% Y_2O_3 [19] and M11, which is the result of a hoop stress because of a tube [9].

MA957 with fine-grains indicates the value a little higher than J1-L [6], and 12YWT indicates the highest value within the data in literatures [20]. However, they, especially 12YWT, show large reduction in strength at longer time as compared with J1-L. It seems that MA957 with fine-grains, 12YWT and J1-L show comparable strength in 100 000 h at 650 °C. On the other hand, it is reported that the uni-axial direction of F4, the ferritic ODS steel, in a form of tube shows high strength and hardly indicates strength reduction at 700 °C [16].

The ferritic ODS steels indicate huge anisotropy in creep strength. For example, although the uni-axial longitudinal stress of F4 is 280 MPa, the hoop strength which is equivalent to the transversal strength is 140 MPa at the time of rupture of 1000 h at 700 °C [16]. On the other hand, the creep strengths of J1-L and J1-T are estimated to be 195 MPa and 164 MPa using Eq. (1) at 1000 h at 700 °C, respectively. That is, the transversal strength of J1 is stronger than the hoop strength of F4 which is a ferritic ODS steel, and the difference of creep strength of J1-L and J1-T is below 20%. If the creep data and the feature of deformation in other ODS steels may be printed, it will greatly contribute to the development of ODS steels through comparative study.

4. Conclusions

Microstructures and creep behavior of 8%Cr–2%W–0.2%V–0.1%Ta (J1) and 8%Cr–1%W (J2) with finely dispersed Y–Ti complex oxide particles, reduced activation ferritic ODS steels, have been investigated and following conclusions have been obtained.

1. Results of creep tests carried out at 670, 700 and 730 °C indicated the time to rupture of J1 was much longer than J2. The time to rupture along the rolling direction was longer than in the transversal direction for J1 and J2. The finely dispersed particles of yttrium and titanium complex oxide existed in J1 and J2. J1 showed low rupture elongation and the shrinkage at the beginning of creep deformation in many cases, and the shrinkage is possibly owing to the formation of finely precipitated TaC particles which is responsible for the high creep strength of J1.
2. Elongated grains of δ-ferrite in the rolling direction existed in J1 and J2 ODS steels in the normalized and tempered condition. Volume fractions of δ-ferrite of J1 and J2 were about 15% and 10%, respectively. The elongated δ-ferrite affects the creep strength and the anisotropy of creep behavior.
3. J1 showed higher creep strength than any other martensitic ODS steels and conventional high strength heat resistant steels. The transversal strength of J1 is stronger than the hoop strength of the ferritic ODS steel cladding, and the anisotropy of creep strength of J1 is relatively small compared with the ferritic ODS steel.

References

[1] K. Shiba, M. Enoeda, S. Jitsukawa, J. Nucl. Mater. 239–333 (2004) 243.
[2] S. Ukai, S. Mizuta, T. Yoshitake, T. Okuda, M. Fujiwara, S. Hagi, T. Kobayashi, J. Nucl. Mater. 283–287 (2000) 702.
[3] R. Schäeublin, T. Leguey, P. Spätig, N. Baluc, M. Victoria, J. Nucl. Mater. 307–311 (2002) 778.
[4] H. Kishimoto, M.J. Alinger, G.R. Odette, T. Yamamoto, J. Nucl. Mater. 329–333 (2004) 369.
[5] H.S. Cho, A. Kimura, S. Ukai, M. Fujiwara, J. Nucl. Mater. 329–333 (2004) 387.
[6] A. Alamo, V. Lambard, X. Averty, M.H. Mathon, J. Nucl. Mater. 329–333 (2004) 333.
[7] S. Ohtsuka, S. Ukai, H. Sakasegawa, M. Fujiwara, T. Kato, T. Narita, J. Nucl. Mater. 367–370 (2007) 160.
[8] S. Ukai, S. Mizuta, M. Fujiwara, T. Okada, T. Kobayashi, J. Nucl. Sci. Technol. 39 (2002) 778.
[9] S. Ukai, T. Kaito, S. Ohtsuka, T. Narita, M. Fujiwara, T. Kobayashi, ISIJ Int. 43 (2003) 2038.
[10] K. Shiba, K. Nakamura, Private communication.
[11] S. Ohtsuka, S. Ukai, M. Fujiwara, T. Kaito, T. Narita, J. Nucl. Mater. 329–333 (2004) 372.
[12] M. Tamura, K. Shinozuka, H. Esaka, S. Sugimoto, K. Ishizawa, K. Masamura, J. Nucl. Mater. 283–287 (2000) 667.
[13] M. Tamura, H. Kusuyama, K. Shinozuka, H. Esaka, ISIJ Int. 47 (2007) 317.
[14] S. Ukai, T. Nishida, H. Okuda, J. Nucl. Sci. Technol. 34 (1997) 256.
[15] M. Tamura, H. Esaka, K. Shinozuka, ISIJ Int. 39 (1999) 380.
[16] S. Ukai, T. Okuda, M. Fujiwara, T. Kobayashi, S. Mizuta, H. Nakashima, J. Nucl. Sci. Technol. 39 (2002) 872.
[17] M. Tamura, H. Sakasegawa, A. Kohyama, H. Esaka, K. Shinozuka, J. Nucl. Mater. 329–333 (2004) 328.
[18] R.L. Klueh, J.P. Shingledecker, R.W. Swindeman, D.T. Hoelzer, J. Nucl. Mater. 341 (2005) 103.
[19] R. Lindau, A. Möslang, M. Schirra, P. Schlossmacher, M. Klimenkov, J. Nucl. Mater. 307–311 (2002) 769.
[20] R.L. Klueh, P.J. Maziasz, I.S. Kim, L. Heartherly, D.T. Hoelzer, N. Hashimoto, E.A. Kenik, K. Miyahara, J. Nucl. Mater. 307–311 (2002) 773.
[21] M. Taneike, F. Abe, K. Sawada, Nature 424 (2003) 294.
[22] T. Horiuchi, M. Igarashi, F. Abe, ISIJ Int. 42 (2002) S67.